ELSEVIER

Journal of Luminescence 90 (2000) 39–48

JOURNAL OF LUMINESCENCE

www.elsevier.com/locate/jlumin

The temperature dependence of energy transfer between the Tm $^3F_4$ and Ho $^5I_7$ manifolds of Tm-sensitized Ho luminescence in YAG and YLF

Brian M. Walsh[a,*], Norman P. Barnes[b], Baldassare Di Bartolo[a]

[a]*Department of Physics, Boston College, Chestnut Hill, MA 02167, USA*
[b]*NASA Langley Research Center, Hampton, VA 23681, USA*

Received 31 August 1999; received in revised form 1 November 1999; accepted 3 November 1999

Abstract

The temperature dependence of the energy transfer process between the Tm $^3F_4$ and Ho $^5I_7$ manifolds in Tm:Ho doped laser materials is investigated. Decay data of luminescence in Tm:Ho:YAG and Tm:Ho:YLF in the temperature range 243–323 K are analyzed to extract energy transfer rates and elucidate the theoretical description of the energy distribution between Tm and Ho ions in solid host materials. © 2000 Elsevier Science B.V. All rights reserved.

PACS: 42.55.P,R; 42.62.F; 42.70.H; 61.72.S

Keywords: Energy transfer; Tm:Ho:YAG; Tm:Ho:YLF; Thulium; Holmium; Tm:Ho lasers

1. Introduction

Due to the efficient energy transfer between Tm $^3F_4$ and Ho $^5I_7$ manifolds, Tm-sensitized Ho materials are used to produce laser action around 2 μm. In these materials Tm is used as a sensitizer or donor, and the laser ion Ho acts as the activator or acceptor. Tm has absorption bands around 790 nm accessible to pumping with diode lasers. In particular, GaAlAs laser diodes, which are also used to pump Nd lasers, are widely available. The absorbed pump radiation in the Tm $^3H_4$ self-quenches to the Tm $^3F_4$, producing 2 Tm atoms in the Tm $^3F_4$ for every photon absorbed into the Tm $^3H_4$. Since the Tm $^3F_4$ and Ho $^5I_7$ manifolds have energy levels that are partially coincident, see Fig. 1, energy can be efficiently transferred from Tm to Ho without the need for phonon assistance. The utility of using diode pumping in conjunction with the 2 for 1 self-quenching, and subsequent Tm → Ho energy transfer, combine to produce a system with attractive features.

In a previous article [1], referred to from here on as article I, we have thoroughly discussed energy transfer in Tm:Ho systems and placed the Tm → Ho energy transfer process within a theoretical framework. In article I, some fundamental principles concerning Boltzmann thermal occupation factors and transition probabilities are incorporated into a set of coupled rate equations describing

* Correspondence address. NASA LaRC, MS 474, Hampton, VA 23681, USA. Tel.: +1-757-864-7112; fax: +1-757-864-8809.

E-mail address: b.m.walsh@larc.nasa.gov (B.M. Walsh)

0022-2313/00/$ - see front matter
PII: S0022-2313(99)00604-3

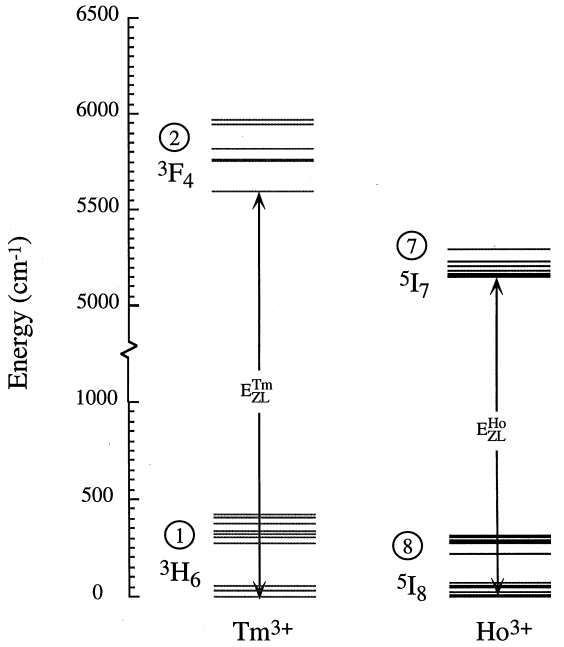

Fig. 1. Energy levels of the two lowest lying manifolds in Tm:Ho:YLF.

rates of change of Tm population in the $^3F_4$ manifold and Ho population in the $^5I_7$ manifold to produce an equation describing the distribution of energy between these manifolds. This result was confirmed using two separate experimental approaches. While this confirmation was pleasing, it involved experiments on only one sample of YAG and one of YLF at room temperature.

In this article, we extend the experimental verification to a third technique in addition to extending the discussion to include a range of dopant ion concentrations and a range of temperatures. These new results correctly track the predicted trends of how the Tm↔Ho distribution should change with temperature and shed some light on the role that phonons may play in the energy sharing. As an additional bonus, this method provides some numerical results for the Tm → Ho and Ho → Tm energy transfer rates and their variation with temperature. These energy transfer rates, used in conjunction with numerical results for branching ratios, cross sections and lifetimes [2], have potential applications for more accurate modeling of Tm:Ho laser systems.

2. Experiment

Temperature control was achieved by placing the samples on a copper plate affixed to a two-stage TE cooler inside a small vacuum chamber with windows to provide an inlet for the pump source and an outlet for the luminescence. The vacuum chamber rested on top of a water-cooled plate to provide a method to carry away the excess heat generated by the TE cooler. The TE cooler offered a temperature variation of -30° to 50°C without the need to change thermistors. The use of a vacuum chamber was needed to prevent condensation and frost on the samples at lower temperatures.

The excitation source used to pump the Tm:Ho samples was a Co:MgF_2 laser, which allowed for the tuning flexibility to optimize pumping of Tm around 1.7 μm or to optimize pumping of Ho around 2.0 μm. This was advantageous since Tm:Ho:YLF and Tm:Ho:YAG have different absorption features, and the Co:MgF_2 laser allowed us to tune to favorable absorption features in these materials. The tuning of the Co:MgF_2 laser was achieved with the use of appropriate dichroic mirrors and a birefringent filter plate. In addition, the Co:MgF_2 laser was also *Q*-switched to provide a pulse width of around 2–5 μs. A small pulse width was needed so as not to obscure the early time portions of the decay profile, where the energy transfer takes place over a time scale of approximately 50–100 μs.

Signal detection was achieved by collecting the luminescence with a lens and focusing it into the entrance slit of a 0.25 m monochromator, with an InSb liquid-nitrogen-cooled detector on the exit slit. Because of the low signal levels due to the use of a monochromator, a preamplifier was necessary. A balance between gain, bandwidth and noise level was obtained that offered an acceptable signal level with a resolution of around 5 μs, compatible with the limitations already imposed by the 5 μs laser pulse width from the Co:MgF_2 laser. The signal from the InSb detector was sent to an oscilloscope for digitization and averaging. The signal was averaged over 512 traces to provide a smooth, relatively low noise signal pattern.

The setup is shown in Fig. 2. Decay patterns were measured from -30° to 50°C in 10°C

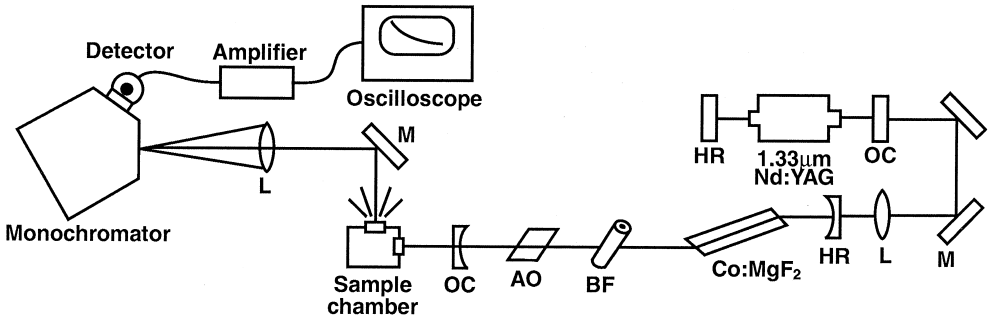

Fig. 2. Experimental apparatus for temperature-dependent decay measurements.

increments. These temperatures were used to obtain Tm $^3F_4$ and Ho $^5I_7$ decay while pumping Tm at 1.7 μm and Ho at 1.9 μm for 4 Tm : Ho : YLF samples, specifically Tm(4)Ho(0.5), Tm(4)Ho(1), Tm(6)Ho(0.5), Tm(6)Ho(1). The two Tm : Ho YAG samples measured were Tm(6)Ho(0.5) and Tm(6)Ho(1). In this notation Tm(A)Ho(B) means A% Tm ions and B% Ho ions of the total number of Y^{3+} sites, which is approximately 1.38×10^{22} ions/cm^3 in both YAG and YLF. The decay patterns acquired by the oscilloscope were saved to disk and taken to a computer for data reduction and analysis.

3. Analysis

In article I we showed that the rate equations governing the rate of change of populations in the Tm $^3F_4$ and Ho $^5I_7$ manifolds could be written, respectively, as

$$\frac{dn_2}{dt} = -\frac{n_2}{\tau_2} - P_{28}C_{Ho}N_s n_2 + P_{71}C_{Tm}N_s n_7 + (P_{28} - P_{71})n_2 n_7, \quad (1)$$

$$\frac{dn_7}{dt} = -\frac{n_7}{\tau_7} + P_{28}C_{Ho}N_s n_2 - P_{71}C_{Tm}N_s n_7 - (P_{28} - P_{71})n_2 n_7, \quad (2)$$

where the subscripts 1, 2, 7, and 8 denote the Tm $^3H_6$, Tm $^3F_4$, Ho $^5I_7$, and Ho $^5I_8$ manifolds, respectively. We use this numbering scheme because in more complicated rate equation models involving other energy transfer processes, such as upconversion and self-quenching, we need to consider some higher lying manifolds, that is, 3 for the Tm $^3H_5$, 4 for the Tm $^3H_4$, 5 for the Ho $^5I_5$, and 6 for the Ho $^5I_6$. P_{28} is the Tm → Ho energy transfer parameter since it involves a nonradiative transfer of energy from an excited Tm $^3F_4$ ion, level 2, to an unexcited Ho $^5I_8$ ion, level 8. Similarly, P_{71} is the Ho → Tm energy transfer parameter since it involves a nonradiative transfer of energy from an excited Ho $^5I_7$ ion, level 7, to an unexcited Ho $^3H_6$ ion, level 1. In addition, C_{Tm} is the thulium concentration, C_{Ho} is the holmium concentration, and N_s is the Y^{3+} site density.

Letting $\alpha = P_{28}C_{Ho}N_s$ and $\beta = P_{71}C_{Tm}N_s$, and linearizing Eqs. (1) and (2) by dropping the terms containing $n_2 n_7$, they can be recast as

$$\frac{dn_2}{dt} = -\frac{n_2}{\tau_2} - \alpha n_2 + \beta n_7, \quad (3)$$

$$\frac{dn_7}{dt} = -\frac{n_7}{\tau_7} + \alpha n_2 - \beta n_7. \quad (4)$$

In linearizing Eqs. (1) and (2) we are considering the low excitation density regime in which $n_2 n_7 \ll N_s C_{Tm} n_2$ or $N_s C_{Ho} n_7$. Since n_2 and n_7 will be small for low excitation densities then their product is very small. In this experiment we had 10 mJ of excitation energy in a spot 2 mm in diameter. This corresponds to an excitation density of 0.5 J/cm^2. This can be considered a low excitation density, so the approximation is valid. More accurately, one can compare the excited manifold density to the total ion density. A simple calculation for

a laser energy of 10 mJ exciting Tm at 1.75 μm in a beam of 2.0 mm diameter shows that approximately 0.5% of the Tm ions are excited. This is at the onset of when the number of Ho excitations becomes nonlinear with the number of Tm excitations. Now, linearizing Eqs. (1) and (2) has the appealing aspect of allowing us to solve Eqs. (3) and (4) in closed form. The solution using Laplace transforms and the approximations used is given in the appendix. The solutions for Tm excitation are

$$\frac{n_2(t)}{n_2(0)} = \left(\frac{\beta}{\alpha+\beta}\right)\exp(-t/\tau) + \left(\frac{\alpha}{\alpha+\beta}\right)\exp[-(\alpha+\beta)t], \quad (5)$$

$$\frac{n_7(t)}{n_2(0)} = \left(\frac{\alpha}{\alpha+\beta}\right)\exp(-t/\tau) - \left(\frac{\alpha}{\alpha+\beta}\right)\exp[-(\alpha+\beta)t], \quad (6)$$

while the solutions for Ho excitation are

$$\frac{n_7(t)}{n_7(0)} = \left(\frac{\alpha}{\alpha+\beta}\right)\exp(-t/\tau) + \left(\frac{\beta}{\alpha+\beta}\right)\exp[-(\alpha+\beta)t], \quad (7)$$

$$\frac{n_2(t)}{n_7(0)} = \left(\frac{\beta}{\alpha+\beta}\right)\exp(-t/\tau) - \left(\frac{\beta}{\alpha+\beta}\right)\exp[-(\alpha+\beta)t]. \quad (8)$$

Eq. (5) can be used to fit experimental decay data in the case of Tm decay when exciting Tm and Eq. (7) can be used to fit experimental decay data in the case of Ho decay when exciting Ho. Eqs. (6) and (8), while still useful, are a little more difficult to handle in that they require a knowledge of the populations at $t = 0$, that is $n_2(0)$ and $n_7(0)$. For instance, Eq. (6), which describes the Ho population as a function of time when exciting Tm, requires a knowledge of the initial excitation population of Tm ions, $n_2(0)$. This is an unknown quantity that can only be approximated. Eq. (5) also appears to require a knowledge of this quantity, but since this equation is of the form $n_2(t)/n_2(0)$, it is simply a matter of normalizing the experimental data since $n_2(t)/n_2(0) = 1$ at $t = 0$. $n_7(t)/n_2(0)$ cannot be handled in this way. Of course, the initial excitation densities, $n_2(0)$ or $n_7(0)$, could be used as a fitting parameter in Eqs. (6) or (8). Therefore, to keep the situation simple with a minimum of fitting parameters, we utilize Eqs. (5) and (7) in this study.

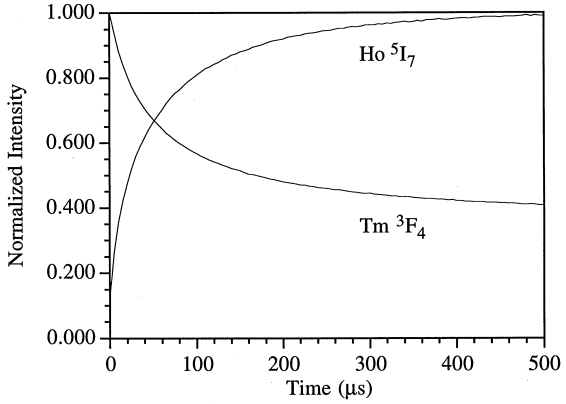

Fig. 3. Experimental decay at early times in Tm:Ho:YLF.

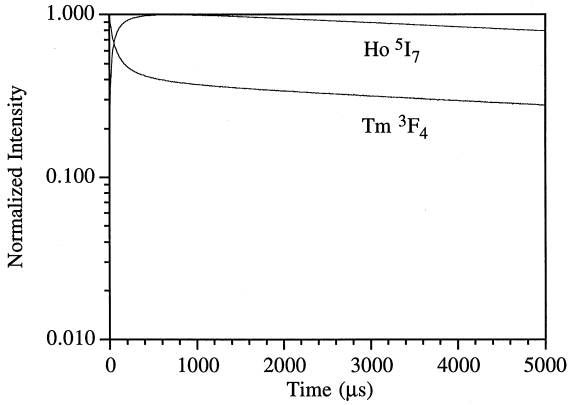

Fig. 4. Experimental decay at later times in Tm:Ho:YLF.

A representative example of the experimental decay of Tm:Ho systems is shown in Figs. 3 and 4. The early time of the decay of Tm(4)Ho(0.5)YLF at 293 K when exciting the Tm $^3F_4$ at 1.75 μm is shown in Fig. 3. Initially there is a fast rise in the

Ho $^5I_7$ accompanied by a fast decay in Tm $^3F_4$. This illustrates the Tm → Ho energy transfer at early times before equillibrium has set in. Fig. 4 shows the same situation on a longer time scale. It is shown in a natural log scale to illustrate that at later times, when thermal equillibrium has set in, the Tm $^3F_4$ and Ho $^5I_7$ manifolds decay at the same rate. At this point the energy transfer is still taking place, but is hidden because the Tm and Ho ions are sharing their excitations in a state of quasi thermal equillibrium such that they decay at the same rate.

At any rate, for Tm decay under Tm excitation we have fit the experimental data from 243 to 323 K for several dopant ion concentrations in YAG and YLF to Eq. (5). For Ho decay under Ho excitation we have used Eq. (7). In the fitting we allowed α, β, and τ to vary until the best fit was obtained. The extracted transfer rates, α and β, were converted into concentration-independent rate constants, P_{28} and P_{71}, using the previously introduced relations $\alpha = P_{28} C_{\mathrm{Ho}} N_s$ and $\beta = P_{71} C_{\mathrm{Tm}} N_s$. We make the distinction here between energy transfer rate and energy transfer parameter. Since the actual rate of transfer between Tm and Ho ions depends on the distance between the ions, then the transfer rate will, in general, depend on dopant concentration. A more useful quantity is the energy transfer parameter, that can be applied to any sample regardless of concentration. So, we call α and β the energy transfer rate of Tm → Ho and Ho → Tm transfer, respectively, to indicate an energy transfer rate with units of μs^{-1}. We call P_{28} and P_{71} the energy transfer parameters of Tm → Ho and Ho → Tm transfer, respectively, to indicate the concentration-independent counterparts with units of $cm^3/\mu s$.

4. Results

In the case of the excitation of the Tm $^3F_4$ manifold, the energy transfer parameters of Tm $^3F_4$ → Ho $^5I_7$, P_{28}, and Tm $^3F_4$ → Ho $^5I_7$ back-transfer, P_{71}, have been plotted versus temperature for four samples of YLF and 2 of YAG. The results are shown in Figs. 5 and 6 for YLF and Figs. 7 and 8 for YAG. As can be seen in these figures,

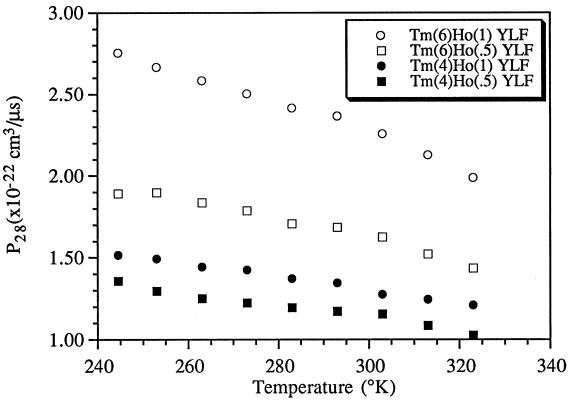

Fig. 5. P_{28} Energy transfer parameter versus temperature in YLF.

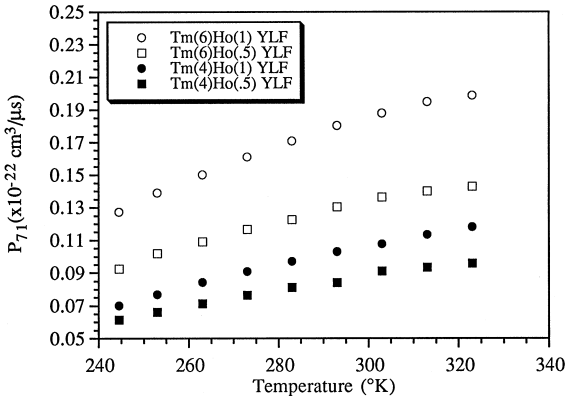

Fig. 6. P_{71} Energy transfer parameter versus temperature in YLF.

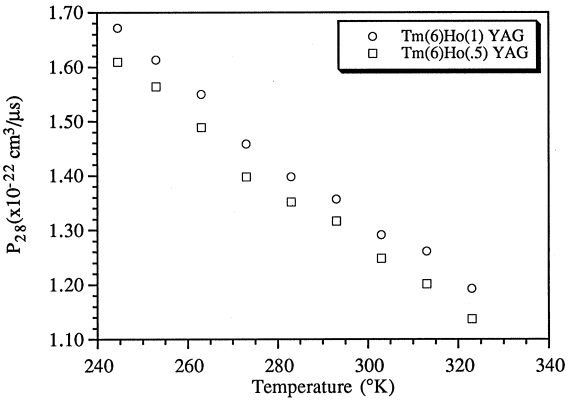

Fig. 7. P_{28} Energy transfer parameter versus temperature in YAG.

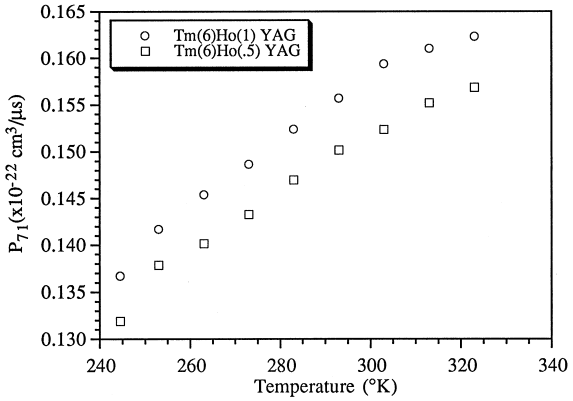

Fig. 8. P_{71} Energy transfer parameter versus temperature in YAG.

there is some spread in the data with sample concentration. The spread is not that severe since the results agree within a factor of 1.5–2.5. So, we may say with a fair amount of confidence that the energy transfer parameters extracted here are good to within a factor of two. Given the difficulty of the experiment and the simple model adopted in addition to the fact that such quantities have previously only been order of magnitude estimates, we consider the results satisfactory. The possibility exists that diffusion among the ions may play some role in contributing to the spread in the data with concentration. The use of more sophisticated models [10,11], which include diffusion, may elucidate this conjecture further.

To see if the energy transfer parameters are acceptable numbers, we investigate their ratio, P_{71}/P_{28}. The core result of article I was a rigorous theoretical derivation of this ratio, the so-called equilibrium constant, $\Theta(T)$, given by the equation

$$\frac{P_{71}}{P_{28}} = \Theta(T) = \frac{Z_2 Z_8}{Z_1 Z_7} \exp[\beta(E_{ZL}^{Ho} - E_{ZL}^{Tm})], \qquad (9)$$

where Z_1, Z_2, Z_7, Z_8 are the partition functions of the Tm $^3H_6$, Tm $^3F_4$, Ho $^5I_7$, and Ho $^5I_8$ manifolds, respectively. $\beta = (kT)^{-1}$, and E_{ZL}^{Ho}, E_{ZL}^{Tm} are the so-called zero-line energies of Ho and Tm, respectively, as shown in Fig. 1. The zero-line energy is the energy difference between the lowest Stark level of the excited manifold and the lowest Stark level of the ground manifold.

The equilibrium constant essentially tells how the Tm and Ho ions are sharing excitation energy. The Tm↔Ho energy sharing is most apparent in the first 50–100 μs of decay. After excitation the Tm and Ho ions have a certain amount of energy as a combined system and an agreement through Boltzmann statistics to maintain the distribution between the two. Even though the total amount of energy in the upper manifolds, Tm $^3F_4$ and Ho $^5I_7$, is decreasing, the distribution between the two eventually reaches quasi thermal equilibrium and the Tm and Ho ions decay at the same rate. By looking at the early parts of the decay curve, we can catch Tm and Ho in the act of sharing their energy.

So, as an indicator of the goodness of our values for P_{28} and P_{71} we compare P_{71}/P_{28} as given theoretically by Eq. (9) with our measured values. Figs. 9 and 10 show P_{71}/P_{28} versus temperature for YLF and YAG, respectively. Despite the fact that the experimental values of P_{28} and P_{71} show some variation with dopant concentration, their ratio shows very little variation with concentration. So, Figs. 9 and 10 represent the average of all P_{71}/P_{28} in YLF and YAG, respectively. The measured ratio shows the same trend of increasing with temperature as the theoretical ratio, but are about 25% larger in both YLF and YAG. A possible explanation for this discrepancy is the following. The theoretical ratio from Eq. (9) considers only those transfer events that are resonant, meaning

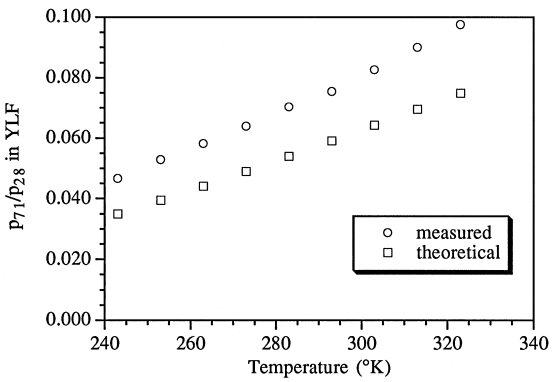

Fig. 9. P_{71}/P_{28} versus temperature in YLF.

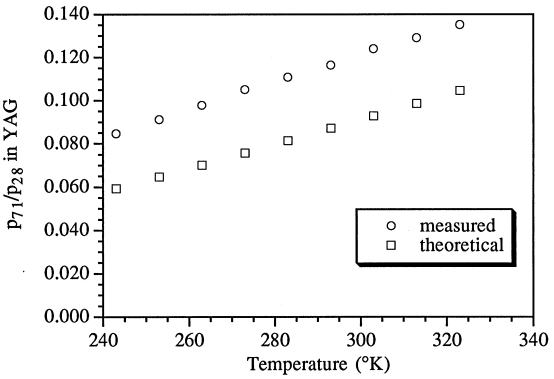

Fig. 10. P_{71}/P_{28} versus temperature in YAG.

that the Stark level difference between levels participating in the transfer in the upper and lower manifolds of Tm and Ho nearly match to within 10 cm^{-1} or so. The measured values may reflect the participation of phonons in the Tm↔Ho transfer such that the nonresonant portions, which require a phonon to conserve energy, effectively act to increase the P_{71}/P_{28} ratio. When energy is transferred from Tm to Ho, the P_{28} process, the excitations in Ho redistribute into the lower Stark levels and cannot transfer back to Tm, the P_{71} process without the assistance of phonons. With the availability of phonons, the P_{71} process can become more prolific because the Tm and Ho energy levels participating in the energy transfer process no longer have to be in resonance. While the P_{28} process benefits from phonon assistance also, the P_{71} process benefits much more. The result is an increase in P_{71}/P_{28} when phonon-assisted processes are included. In fact, the reason the P_{71}/P_{28} process increases with temperature is because the higher lying Stark levels in Ho become more populated and the P_{71} backtransfer becomes larger. Although the temperature range examined was only about 80 K, Figs. 9 and 10 show a subtle, but consistent increasing difference between measured and theoretical P_{71}/P_{28} ratios in the temperature range 243 to 323 K. This adds support to our assumption of the contribution of phonon assisted transfer events since at higher temperatures the higher energy phonon modes become available and the observed difference between measurement and resonant theory should become larger. In Table 1 we have tabulated measured rate parameters, P_{28} and P_{71} from the literature and this study for comparison.

In article I we measured P_{71}/P_{28} at room temperature using two different experimental techniques that differ from the one used here. The details of those experimental techniques are given in article I. We refer to P_{71}/P_{28} as measured in article I as Θ_1 and Θ_2, the P_{71}/P_{28} measured here as Θ_3, and the theoretical value from Eq. (9) as Θ_t. The results are tabulated in Table 2 for YAG and YLF. Three separate experiments give values of Θ that are slightly higher than that predicted by theory. This is an indication that the theoretical expression for P_{71}/P_{28} in Eq. (9) is at best a lower limit on the ratio. The actual case is estimated to be

Table 1
Values for energy transfer parameters in Tm:Ho:YAG and Tm:Ho:YLF at room temperature

Material	P_{28} ($cm^3/\mu s$)	P_{71} ($cm^3/\mu s$)	P_{71}/P_{28}	Reference
YAG	$0.7–2.2\times10^{-22}$	–	–	[3]
YAG	1.3×10^{-22}	1.0×10^{-23}	0.0769	[4]
YAG	2.0×10^{-22}	2.5×10^{-23}	0.1270	[5]
YAG	1.0×10^{-22}	1.0×10^{-23}	0.1000	[6]
YAG	7.8×10^{-22}	8.0×10^{-23}	0.0975	[7]
YAG	3.2×10^{-22}	–	–	[8]
YAG	1.3×10^{-22}	1.5×10^{-23}	0.1165	This study
YLF	$0.5–1.5\times10^{-22}$	–	–	[3]
YLF	8.3×10^{-23}	1.0×10^{-23}	0.1204	[7]
YLF	7.4×10^{-23}	–	–	[8]
YLF	6.0×10^{-23}	8.3×10^{-24}	0.1383	[9]
YLF	$1.2–2.3\times10^{-22}$	$0.9–1.9\times10^{-23}$	0.0755	This study

Table 2
Values for the equilibrium constant in YAG and YLF at room temperature

Material	Θ_t	Θ_1	Θ_2	Θ_3
YAG	0.0911	0.1049	0.1000	0.1165
YLF	0.0621	0.0735	0.0719	0.0755

approximately 25% higher in the vicinity of room temperature, that is 300 ± 50 K.

5. Fractional populations

Assuming that all the excitation resides in the Tm $^3F_4$ and Ho $^5I_7$ manifolds, it was shown in article I that the fraction of Ho ions residing in the $^5I_7$ manifold is

$$f_{\mathrm{Ho}} = \frac{C_{\mathrm{Ho}}(Z_7/Z_8)\exp(-\beta E_{\mathrm{ZL}}^{\mathrm{Ho}})}{C_{\mathrm{Ho}}(Z_7/Z_8)\exp(-\beta E_{\mathrm{ZL}}^{\mathrm{Ho}}) + C_{\mathrm{Tm}}(Z_2/Z_1)\exp(-\beta E_{\mathrm{ZL}}^{\mathrm{Tm}})} \quad (10)$$

while the fraction residing in the Tm $^3F_4$ manifold is then $f_{\mathrm{Tm}} = 1 - f_{\mathrm{Ho}}$.

As was pointed out in article I, these expressions for the fractional populations differ from those which are widely used in the literature [4,12–14]. The reason for this discrepancy is that fractional populations have traditionally been derived on the basis of Castleberry's [15] theory, which is inconsistent with experimental and theoretical observations. We stress that the fractional populations calculated in this way are only accurate when low excitation densities are utilized in the experiment and should not be used in cases where the excitation density is high enough to cause nonlinearity in the number of Ho excitations versus Tm excitations.

In Fig. 11, Eq. (10) is used to plot the fraction of excitations in Tm : Ho : YLF at thermal equilibrium residing in Ho, f_{Ho}, versus temperature for ratios of Tm to Ho concentrations ranging from 2 to 12. The fractional Ho population can also be expressed in terms of the measured energy transfer rates, α and β. The fractional population of the Ho $^5I_7$ manifold can be written as

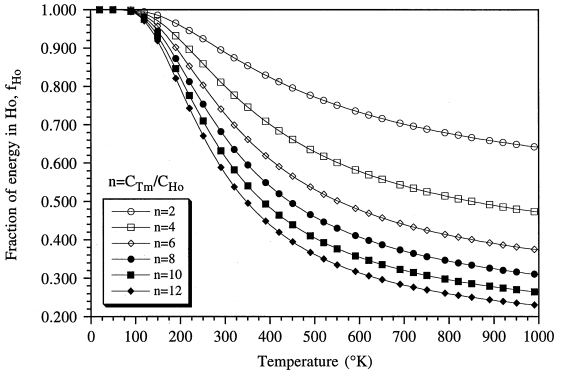

Fig. 11. Predicted fractional Ho population, f_{Ho}, versus temperature for various Tm : Ho concentration ratios (0–1000 K).

$$f_{\mathrm{Ho}} = \frac{1}{1 + n_2/n_7}. \quad (11)$$

Dividing the closed-form solutions for n_2 by n_7 given by Eqs. (5) and (6) and taking $1/\tau \ll \alpha + \beta$, since τ is very long (ms) compared to the energy transfer rates α and β (μs), we find f_{Ho} as a function of time

$$f_{\mathrm{Ho}}(t) = \frac{\alpha}{\alpha + \beta}[1 - \mathrm{e}^{-(\alpha+\beta)t}]. \quad (12)$$

At thermal equilibrium, $t = t_{\mathrm{eq}}$, the exponential term in the above equation is essentially zero since t_{eq} ranges from approximately 200 μs for a Tm/Ho concentration ratio of $n = 12$ to over 1000 μs for $n = 2$. So, essentially we have the result

$$f_{\mathrm{Ho}}(t_{\mathrm{eq}}) \simeq \frac{\alpha}{\alpha + \beta}. \quad (13)$$

The fraction of energy in Tm : Ho : YLF residing in Ho, f_{Ho}, at thermal equilibrium versus temperature in the range 230–330 K for Tm/Ho concentration ratios of 4, 6, 8, and 12 is plotted in Fig. 12. The solid lines represent the theoretical results from Eq. (10), while the dashed lines represent the experimental results using Eq. (13) and the extracted energy transfer rates α and β from fitting Eqs. (5) and (6) to experimental decay curves. In this

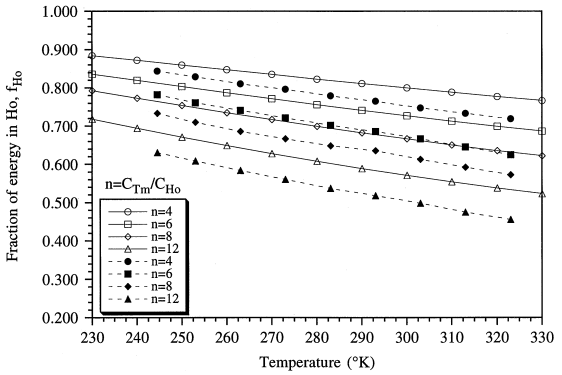

Fig. 12. Predicted and measured fractional Ho population, f_{Ho}, versus temperature for various Tm : Ho concentration ratios (230–330 K).

figure, $n = 4$ represents Tm(4)Ho(1) YLF, $n = 6$ is Tm(6)Ho(1) YLF, $n = 8$ is Tm(4)Ho(0.5) YLF, and $n = 12$ is Tm(6)Ho(0.5) YLF. As can be seen from this graph, the agreement is quite good, with a difference between experiment and theory of less than 10%. These graphs indicate that to maximize the energy storage in Ho the Tm/Ho concentration ratio should be minimized. For example, if 6% is chosen for the Tm donor concentration then a Ho acceptor concentration of 1.0% would offer 30% more storage than a Ho acceptor concentration of 0.5%. Ho concentrations less than 1.0% are often used in Tm : Ho materials for lasing around 2.0 μm, but as Fig. 8 shows, adding more holmium could be beneficial if up-conversion from the the lasing manifold to higher manifolds in Ho is not a concern.

6. Conclusions

The temperature dependence of the energy transfer process between the Tm $^3F_4$ and Ho $^5I_7$ manifolds in Tm : Ho-doped YAG and YLF has been investigated. The decay dynamics, under excitation by a Q-switched Co : MgF_2 laser, in four YLF samples and two YAG samples of various Tm : Ho concentrations were examined in the temperature range 240–330 K. For Tm decay under Tm excitation, we have fit the experimental decay data from 243 to 323 K for several dopant ion concentrations in YAG and YLF to Eq. (5). The extracted fitting parameters provide numerical results for the Tm → Ho and Ho → Tm energy transfer rates and their variation with temperature. The results correctly track the predicted trends of how the Tm↔Ho distribution should change with temperature.

With the addition of the experimental results presented in this article, we now have three independent experimental measurements of the Tm : Ho equilibrium constant, $\Theta(T)$. The current method has provided measurements for the variation of Tm : Ho ion concentrations and temperature as well. The results consistently show, that in all of these experimental methods, the measured values are approximately 25% higher than the theory of the energy distribution predicts. This may be an indication of the role that phonons play in the energy transfer dynamics.

In the final section, we have presented theoretical expressions for fractional populations of Tm and Ho of the total number of excitations in the coupled Tm–Ho system, which differ from those which are widely used in the literature. Experimental results for the fractional populations based on measured energy transfer rates are compared with the theoretical calculations. Agreement is seen to be better than 10%.

Acknowledgements

The authors wish to acknowledge the sponsorship of this work by NASA grant NAG-1-2057. One of the authors would like to thank W.J. Rodriquez and D.J. Reichle for their assistance in assembling the Co : MgF_2 laser.

Appendix

Taking the Laplace transform of Eqs. (3) and (4) leads to,

$$sn_2(s) - n_2(0) = -\frac{n_2(s)}{\tau_2} - \alpha n_2(s) + \beta n_7(s), \quad \text{(A.1)}$$

$$sn_7(s) - n_7(0) = -\frac{n_7(s)}{\tau_7} + \alpha n_2(s) - \beta n_7(s). \quad \text{(A.2)}$$

In the case of Tm excitation, $n_7(0) = 0$ since initially at $t = 0$ there are no excitations in Ho. All the initial excitation resides in Tm only. Taking $n_7(0) = 0$ and combining Eqs. (10) and (11) gives

$$n_2(s) = \frac{s + \frac{1}{2}(1/\tau_7 + \beta) - \frac{1}{2}(1/\tau_2 + \alpha)}{s^2 + (1/\tau_2 + 1/\tau_7 + \alpha + \beta)s + (1/\tau_2\tau_7 + \beta/\tau_2 + \alpha/\tau_7)} \times n_2(0). \quad (A.3)$$

Completing the square on the denominator and rearranging, Eq. (A.3) can be written as

$$n_2(s) = \frac{s + 1/\tau_2}{(s + a)^2 + b^2} n_2(0), \quad (A.4)$$

where

$$a = \tfrac{1}{2}(1/\tau_2 + 1/\tau_7 + \alpha + \beta) \quad (A.5)$$

and

$$b^2 = (1/\tau_2\tau_7 + \beta/\tau_2 + \alpha/\tau_7) - \tfrac{1}{4}(1/\tau_2 + 1/\tau_7 + \alpha + \beta)^2. \quad (A.6)$$

Taking the inverse Laplace transform, Eq. (A.4) becomes

$$\frac{n_2(t)}{n_2(0)} = \exp(-at)\cos(bt) + \frac{1}{2b}(1/\tau_7 - 1/\tau_2 + \beta - \alpha)\exp(-at)\sin(bt). \quad (A.7)$$

Expanding the squared term in Eq. (A.6), collecting terms and solving for b, we find

$$b = \pm \mathrm{i}[\tfrac{1}{4}(1/\tau_2 - 1/\tau_7)^2 + \tfrac{1}{4}(\alpha + \beta) + \tfrac{1}{2}(\alpha - \beta)(1/\tau_2 - 1/\tau_7)]^{1/2}. \quad (A.8)$$

For thermal equilibrium $\tau \simeq \tau_2 \simeq \tau_7$ and the first and third terms in b disappear. We are left with

$$a \simeq 1/\tau + \tfrac{1}{2}(\alpha + \beta), \quad (A.9)$$

$$b \simeq \pm \tfrac{1}{2}\mathrm{i}(\alpha + \beta). \quad (A.10)$$

The solution in Eq. (A.7), with $\tau_2 \simeq \tau_7$ becomes

$$\frac{n_2(t)}{n_2(0)} = \exp\left[-\left(\frac{1}{\tau} + \frac{\alpha + \beta}{2}\right)t\right] \times \left[\cos\left(\mathrm{i}\frac{\alpha + \beta}{2}t\right) + \mathrm{i}\frac{\alpha - \beta}{\alpha + \beta}\sin\left(\mathrm{i}\frac{\alpha + \beta}{2}t\right)\right] \quad (A.11)$$

Using the Euler equation, $\exp(\mathrm{i}\theta) = \cos(\theta) + \mathrm{i}\sin(\theta)$, we arrive at

$$\frac{n_2(t)}{n_2(0)} = \left(\frac{\beta}{\alpha + \beta}\right)\exp(-t/\tau) + \left(\frac{\alpha}{\alpha + \beta}\right) \times \exp[-(\alpha + \beta)t] \quad (A.12)$$

which is Eq. (5).

References

[1] B.M. Walsh, N.P. Barnes, B. Di Bartolo, J. Lumin. 75 (1997) 89.
[2] B.M. Walsh, N.P. Barnes, B. Di Bartolo, J. Appl. Phys. 83 (1998) 2772.
[3] A.A. Nikitichev, OSA Proc. ASSL 24 (1995) 498.
[4] S.R. Bowman, M.J. Winings, R.C.Y. Auyeung, J.E. Tucker, S.K. Searles, B.J. Feldman, IEEE J. Quant. Electron. 27 (1991) 2142.
[5] R. Petrin, M. Jani, R.C. Powell, Opt. Mater. 1 (1992) 111.
[6] G. Armagan, B.M. Walsh, N.P. Barnes, E.A. Modlin, A.M. Buoncristiani, OSA Proc. ASSL 20 (1994) 141.
[7] N.P. Barnes, E.D. Filer, C.A. Morrison, C.J. Lee, IEEE J. Quant. Electron. 32 (1996) 92.
[8] D. Bruneau, S. Delmonte, J. Pelon, Appl. Opt. 37 (1998) 8406.
[9] M. Falconieri, A. Lanzi, G. Salveti, A. Toncelli, Appl. Phys. B 66 (1998) 153.
[10] A. Brenier, G. Boulon, C. Pedrini, J. Lumin. 54 (1993) 271.
[11] L.A. Diaz-Torres, O. Barbosa-Garcia, M.A. Meneses-Nava, C.W. Struck, B. Di Bartolo, Proceedings of Advances in Energy Transfer Processes, International School of Atomic and Molecular Spectroscopy, Erice, Sicily, 1999.
[12] T.Y. Fan, G. Huber, R.L. Byer, P. Mitzscherlich, IEEE J. Quant. Electron. 24 (1988) 924.
[13] M.E. Storm, IEEE J. Quant. Electron. 29 (1993) 440.
[14] J.M. Sousa, J.R. Salcedo, V.V. Kuzmin, Appl. Phys. B 64 (1997) 25.
[15] D.E. Castleberry, Ph.D. Thesis, Massachusetts Institute of Technology, Cambridge, MA, 1975.